scientific reports

Check for updates

OPEN

Identification, characterization, and function analysis of the VIT family in *Phaeodactylum tricornutum*

Rui Zhai[1,2,3], Xiangrui Zhang[4], Shuying Wang[3], Shuai Chen[5], Zhiqi Zhang[4], Yuhan Zhang[4], Dunwen Shi[3], Xinshu Li[1,2,3], Futian Li[1,2,3], Guoqiang Chen[1,2,4]✉ & Juntian Xu[1,2,3]

Iron is an essential microelement for all living organisms. The vacuolar iron transporters (VIT) gene family is found in various species, including yeast, fungi, protozoa, and plants, where it plays a crucial role in sequestration, homeostasis, and tolerance of the heavy metals, particularly iron and manganese. However, the presence and function of VIT genes in marine phytoplankton have not been previously reported. The study aims to identify the VIT family within the marine diatom *Phaeodactylum tricornutum* and to analyze the function of these genes. We conducted a comprehensive analysis of the VIT genes in *P. tricornutum* genome, examining their phylogenetic relationship, physicochemical properties, gene structures, conserved motifs, domains, expression profile, and cis-acting elements using in silico methods. Function analysis were performed through complementation experiments and the expression of eGFP fusion protein in yeast. Four members of the VIT family were identified in *P. tricornutum*. All belonging to the VTL (VIT like) group in phylogenetic tree and containing a VIT1 domain. These genes are distributed across chromosomes 2, 4, and 13, with tandem duplication of the *PtVTL1* and *PtVTL2* contributed to the expansion of this gene family. Expression profile showed that the *PtVTL3* is induced to express highly under light condition, others are induced to express highly under dark. *PtVTL2* is highly induced to express at low Fe condition, and *PtVTL3* is highly induced to express at high Fe condition. Analysis of cis-acting regulatory elements indicated that these genes are primarily involved in responses to environmental stress and phytohormones. Heterologous expression of *PtVTL3* successfully rescued the iron-sensitive phenotype in yeast mutant △*ccc1*. The expression of eGFP-PtVTL3 fusion protein in yeast demonstrated that PtVTL3 is located to the tonoplast. These findings suggest that PtVTL3 function to transport Fe^{2+} across the tonoplast into the vacuole, thereby maintaining iron homeostasis in yeast. Four *PtVTL* genes were identified in the genome of *P. tricornutum*, with PtVTL3 playing a key role in iron transport at the tonoplast, highlighting its potential significance in iron homeostasis in marine diatoms.

Keywords *Phaeodactylum tricornutum*, Vacuolar iron transporter, VIT-like, Iron, Tonoplast

Abbreviations

VIT	Vacuole iron transporter
VTL	VIT-like
ZIP	ZRT, IRT-like protein
ISIP2A	Iron starvation-induced protein 2 A
HMM	Hidden Markov model
CDD	Conserved domain database
ML	Maximum likelihood
TMDs	Transmembrane domains
SD-Ura	SD medium without uracil

[1]Jiangsu Provincial Key Laboratory of Marine Biotechnology, Jiangsu Ocean University, Lianyungang 222005, China. [2]Co-Innovation Center of Jiangsu Marine Bio-industry Technology, Jiangsu Ocean University, Lianyungang 222005, China. [3]School of Marine Science and Fisheries, Jiangsu Ocean University, Lianyungang 222005, China. [4]College of Ocean Food and Biological Engineering, Jiangsu Ocean University, Lianyungang 222005, China. [5]College of Veterinary Medicine, Yangzhou University, Yangzhou 225009, China. ✉email: gqchen@jou.edu.cn

SGR	SD-Ura medium containing 2% galactose and 1% raffinose
EV	Empty vector
eGFP	Enhanced green fluorescent protein
FPKM	Fragments per kilobase of exon per million mapped reads

Iron (Fe) is a crucial micronutrient that serves as an essential cofactor in various biological processes, including photosynthesis, nucleotide biosynthesis, electron transport chains, and nitrogen fixation. It is often a limiting factor for photosynthetic productivity, biomass accumulation, and the community structure of phytoplankton[1,2]. However, the growth of phytoplankton can be significantly hindered by the low bioavailability of iron, particularly in one-third of the open ocean[3,4]. In surface seawater, the majority of iron exists as insoluble organic complex, while dissolved unchelated inorganic iron is at exceedingly low concentration[5].

In the marine diatom *Phaeodactylum tricornutum*, there are three proposed pathways for iron acquisition from ocean[6,7]. First, un-chelated ferric irons can be concentrated at the cell surface and subsequently transported via endocytosis after binding to the phototransferrin iron starvation-induced protein 2 A (ISIP2A)[8,9]. ISIP2A, which possessed carboxylate iron-binding domains, was initially identified in *P.tricornutum*[10], and is localized to both the outer membrane and internal vesicles. A deficiency in ISIP2A impedes high-affinity iron uptake in *P.tricornutum*, though uptake can be restored through complementation with human transferrin[9]. Second, ferric irons complexed with hydroxamate siderophores can bind to the cell surface protein FBP1 (ferrichrome-binding protein) and are transported via endocytosis in a process depended on ISIP1 into the cytosol[11,12]. Third, ferrous iron may be directly taken up by divalent metal transporters belonging to the ZRT/IRT-like protein (ZIP) family, which were identified in *P.tricornutum* genome through homologous genes related to yeast and plant ferrous ion transporters (ZIP family), however, experimental validation for this pathway is still lacking[7,10,13].

In vivo, ferritin and vacuoles serving as the two primary sites for long-term iron storage in most plants[14,15]. Overexpression of ferritin in *P. tricornutum* has been shown to induce a morphological transformation from fusiform to ovoid forms, exhibiting characteristics typical of resting cells and benthic adaption, including reduced growth rates, limited light adaption ability, and silicified valves[16]. Additionally, the vacuole can function as heavy metal repositories for ion homeostasis, necessitating a variety of metal transporters, such as vacuole iron transporter (VIT) and VIT-like (VTL) gene family, as well as Na^+/H^+ antiporters, Mn^{2+} transporters, Copper transporter COPT5, metal transporter proteins (MTPs), cation exchangers (CAXs), heavy metal ATPases (HMA), natural resistance-associated macrophage proteins (NRAMPs), ABC transporter, etc[17–19]. However, it remains undocumented whether specific iron transporters exist in *P. tricornutum* for vacuole sequestration to regulate the iron homeostasis.

In the present study, we identified four genes encoding for vacuolar iron transporters of the VIT, the vacuolar iron transporter gene family, firstly in the *P. tricornutum* genome using in silico approaches. We explored the phylogeny, chromosome distribution, conserved domains, subcellular localization, with a particular focus on the functional analysis of PtVTL3. The findings from this research will enhance our understanding of the regulation mechanism of VIT in *P. tricornutum*.

Methods

Identification and characterization of vacuolar iron transporter (VIT) genes from the *Phaeodactylum tricornutum* genome

To identify potential VIT genes in the *P. tricornutum* genome, we downloaded the Hidden Markov Model (HMM) profile of the VIT domain (PF01988) from the Pfam database (http://pfam.xfam.org/). This profile was used as a query to perform HMMsearch[20] on the *P. tricornutum* genome obtained from the Ensembl Protists database (E value < 1.0 E-5) (http://protists.ensembl.org/). Redundant sequences were eliminated and verified by three protein structure databases: CDD (https://www.ncbi.nlm.nih.gov/cdd), HMMER (https://www.ebi.ac.uk/Tools/hmmer/) and SMART (http://smart.embl.de/).

The Expasy ProtParam tool (https://web.expasy.org/cgi-bin/protparam/protparam) was utilized to analyze the basic physicochemical property of the *PtVIT* genes, including the number of amino acids, molecular weight, and the isoelectric point. Transmembrane domain predictions were conducted using the TMHMM – 2.0 online program (https://services.healthtech.dtu.dk/services/TMHMM-2.0/)[21].

The signal peptides of PtVTLs were predicted by SignalP-4.1 online program (https://services.healthtech.dtu.dk/services/SignalP-4.1/), and the subcellular localization of PtVTLs were predicted by TargetP-2.0 online program (https://services.healthtech.dtu.dk/services/TargetP-2.0/).

Phylogenetic analysis of PtVITs

To investigate the phylogenetic relationship between PtVITs and other plant VITs, we collected 93 VIT amino acid sequences from 12 species, including those from *P. tricornutum* (4), *Oryza sativa* (7), *Arabidopsis thaliana* (6), *Chlamydomonas reinhardtii* (4), *Selaginella moellendorffii* (10), *Zea mays* (7), *Populus trichocarpa* (8), *Physcomitrella patens* (5), *Vitis vinifera* (7), *Glycine max* (21), *Medicago truncatula* (13) and *Saccharomyces cerevisiae* (1). These sequences were sourced from following databases: JGI, Ensembl, RGAP, TAIR and UniPort, and extracted the conserved domain sequences to construct a phylogenetic tree using the maximum likelihood (ML) method in MEGA 7.0[22], with a bootstrap value set at 1000. The *Saccharomyces cerevisiae* CCC1 sequence (P47818)[23–25] served as the outgroup for rooting the tree. The resulting phylogenetic tree was visualized using the iTOL online tool (https://itol.embl.de/)[26].

Conserved motifs, domains, and gene structure of PtVITs

The phylogenetic tree of PtVITs conserved domain amino acid sequences was constructed using the ML method in MEGA 7.0. Conserved motifs and domains were predicted using the MEME online program (suite 5.5.2)

(https://meme-suite.org/meme/tools/meme) with a p value < 0.05[27], as well as the CDD protein structure database with a similar p value threshold[28]. The genome annotation file for *P. tricornutum* was downloaded from the Ensembl database and visualized using TBtools[29].

Chromosome distribution, and gene duplication pattern of *PtVIT* genes

Chromosome distribution data of *PtVIT* genes were extracted from the *P. tricornutum* genome annotation file and visualized using the MG2C v2.1 online program (http://mg2c.iask.in/mg2c_v2.1/)[30]. The Simple Ka/Ks Calculator in TBtools software was utilized for analyzing the gene duplication pattern.

Cis-acting regulatory elements and expression profile of *PtVIT* genes

The 500 bp DNA sequences upstream of the initiation codon of *PtVIT* gene were extracted from the *P. tricornutum* genome using TBtools software[29], subsequently, cis-acting regulatory elements of the promoters were identified using the PlantCARE database (http://bioinformatics.psb.ugent.be/webtools/plantcare/html/)[31], and visualized with GraphPad Prism version 8.3.0 (GraphPad Software, San Diego, California, USA, www.graphpad.com).

Based on the transcriptome data provided in the literature[32], the expression profile of *PtVTL* genes at diel light cycling under iron limitation was studied. The values of FPKM (fragments per kilobase of exon per million mapped reads) were calculated as log2 values, and the expression data were normalized and viewed using the TBtools software[29].

Functional analysis of PtVITs

To investigate the functions of PtVITs, we cloned the genes from *P. tricornutum* into yeast expression vectors for the complementary assay and the subcellular location study.

Total RNA was extracted from the *P. tricornutum* strain CCMA 106, sourced from the State Key Laboratory of Marine Environmental Science of Xiamen University, using the HiPure Plant RNA Mini Kit (Magen, Guangzhou, China). Reverse transcription and RT-PCR were performed using the corresponding primers (Supplementary Table 1), employing a reverse transcription kit and Fast*Pfu* DNA polymerase (TransGen Biotech, Beijing, China). The *PtVTLs* genes were inserted into the yeast expression vector pYES2 using the ClonExpress II One Step Cloning Kit (Vazyme, Nanjing, China).

The recombinant plasmids were transferred into the yeast wild type yeast strain DY150 and into the mutant strains △*ccc1*, △*smf1*, △*Zrt1Zrt2* using the PEG/LiAc method. Positive clones were selected on solid SD medium lacking uracil (SD-Ura) (WEIDI, Shanghai, China), and cultured in glucose-containing SD-Ura liquid medium until the logarithmic growth phase. After centrifugation at 2000 g for 1 min, cell pellets were washed twice with sterile ultrapure water, resuspended in sterile ultrapure water to an OD_{600} of approximately 1, and then two microliters of the cell suspension were spotted on SGR medium (SD-Ura plates containing 2% galactose and 1% raffinose) (WEIDI, Shanghai, China) in four serial 10-fold dilutions. Plates were incubated at 30 ℃ for 2–4 days and subsequently imaged.

The *eGFP* (enhanced Green Fluorescent Protein) gene was synthesized by Sangon Biotech Co., Ltd (Shanghai, China) (no stop codon) and fused with *PtVTL3* gene into the pYES2 vector using the ClonExpress MultiS One Step Cloning Kit (Vazyme, Nanjing, China). The recombinant vector was transformed into yeast mutant strain △*ccc1* via the PEG/LiAc method. Cultures were grown in SD-Ura liquid medium containing 2% galactose and 1% raffinose (WEIDI, Shanghai, China), and incubated with 10 μM of the vacuolar membrane fluorescence dye FM4-64 (Coolaber Technology Co., Ltd., Beijing, China) for 0.5 h at room temperature. The recombinant yeast was imaged using a laser confocal microscope (Leica, Germany).

Results

Identification and characterization of the VIT family in *Phaeodactylum tricornutum*

Using the Hidden Markov model (HMM) profile of the VIT1 (PF01988) via HMMsearch, we identified four putative VIT family genes in the *P. tricornutum* genome. These findings were subsequently validated through three protein structure databases: CDD, SMART and HMMER. The different physiochemical properties of these genes are detailed in Table 1. The results indicated that the four genes are distributed across chromosomes: 2, 4, and 13, and the lengths of the deduced amino acid sequences varied from 280 to 318 residues, with molecular weights ranging from 30 to 34 kD. The number of transmembrane domains (TMD) ranged from 3 to 5.

The signal peptides were predicted by SignalP-4.1 online program, and the results showed that there are not any signal peptides in PtVITs. The subcellular localization of PtVITs were predicted by TargetP-2.0 online program and the results showed that they didn't exist at mitochondria, chloroplast or thylakoid luminal. Therefore, they should be localized at other subcellular organ (Supplementary Table 2).

Gene ID	name	Chromosome position	CDS	Protein	MW (KD)	pI	No. of TMD
Phatr3_J43313	*PtVTL1*	2: 92,426–93,337	912 bp	303aa	32.142	4.492	5
Phatr3_J43314	*PtVTL2*	2: 94,109–95,235	939 bp	312aa	32.854	4.244	4
Phatr3_J26157	*PtVTL3*	4: 735,680–736,522	843 bp	280aa	30.544	4.38	3
Phatr3_J37632	*PtVTL4*	13:583155–584,111	957 bp	318aa	33.851	6.457	5

Table 1. Basic information of VITs in *Phaeodactylum tricornutum*.

Phylogenetic analysis of PtVITs

We collected a total of 93 VIT protein sequences (Supplementary Table 3) and extracted the domain sequences to perform multiple sequences alignment in Mega 7.0 and construct a phylogenetic tree by the ML method. The tree revealed two distinct groups: the VIT group and the VTL group (Fig. 1). The VIT group showed a closer relationship to *Saccharomyces cerevisiae* CCC1 and included characterized ferrous iron transporters such as OsVIT1, OsVIT2[33], AtVIT1[34]. In contrast, the VTL group was larger and comprised many uncharacterized members of the protein family, along with various ferrous iron transporters, including AtVTL1, AtVTL2, AtVTL5[35], MtVTL4, MtVTL8[36], GmVTL1a, and GmVTL1b[37]. Notably, all the four members of VIT family from *P. tricornutum* clustered within the VTL clade. Consequently, based on the chromosomal distribution and phylogenetic relationship, we designated *Phatr3_J43313*, *Phatr3_J43314*, *Phatr3_J26157* and *Phatr3_J37632* as *PtVTL1*, *PtVTL2*, *PtVTL3 and PtVTL4* respectively. Moreover, the phylogenetic analysis indicated that the

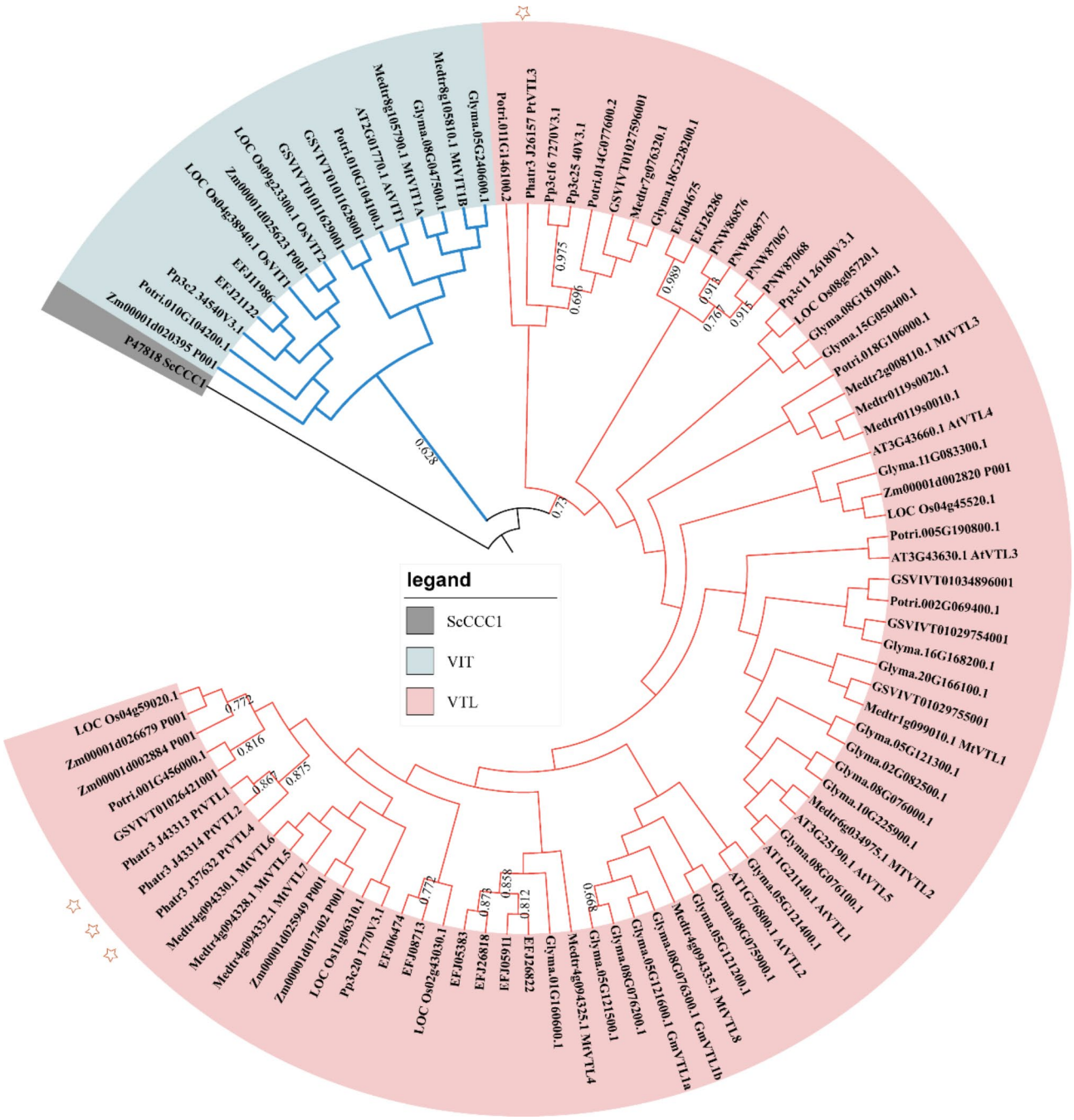

Fig. 1. The phylogenetic tree of PtVTLs basis on their protein domain sequences by ML method. ScCCC1 is used as outgroup. The red clade means the VTL group, and the blue clade represents the VIT group. Red asterisk represented the PtVTLs.

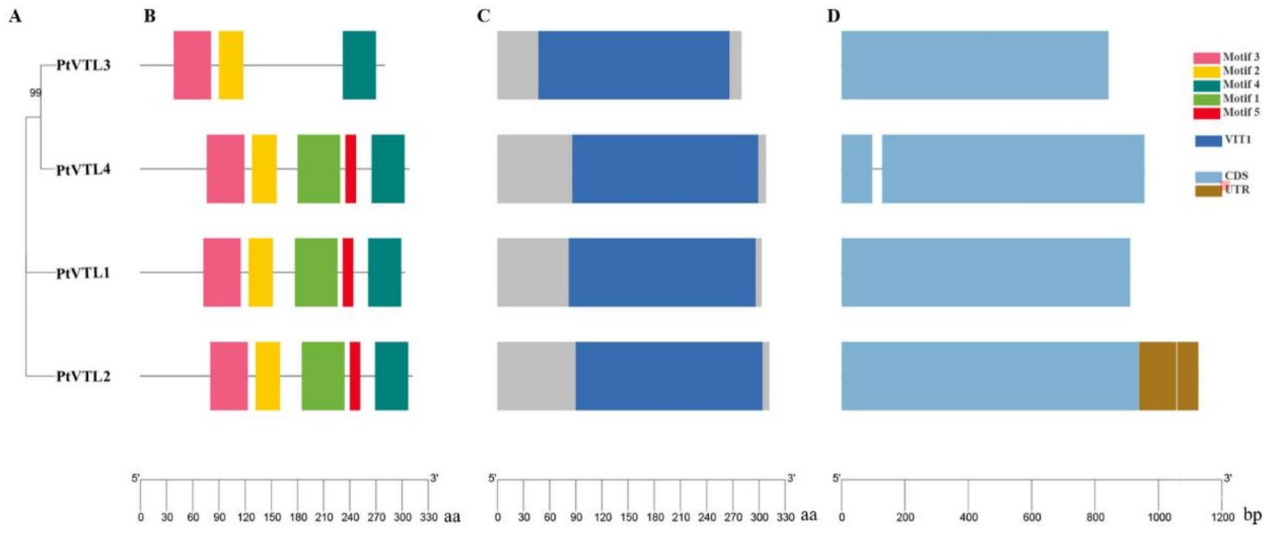

Fig. 2. Phylogenetic tree, conserved motifs, domains and gene structure of PtVTLs. (**A**) the ML phylogenetic tree of PtVTLs based on the protein sequences. (**B**) The conserved motifs of PtVTLs. (**C**) The conserved domain of PtVTLs. (**D**) the gene structure of *PtVTL* genes.

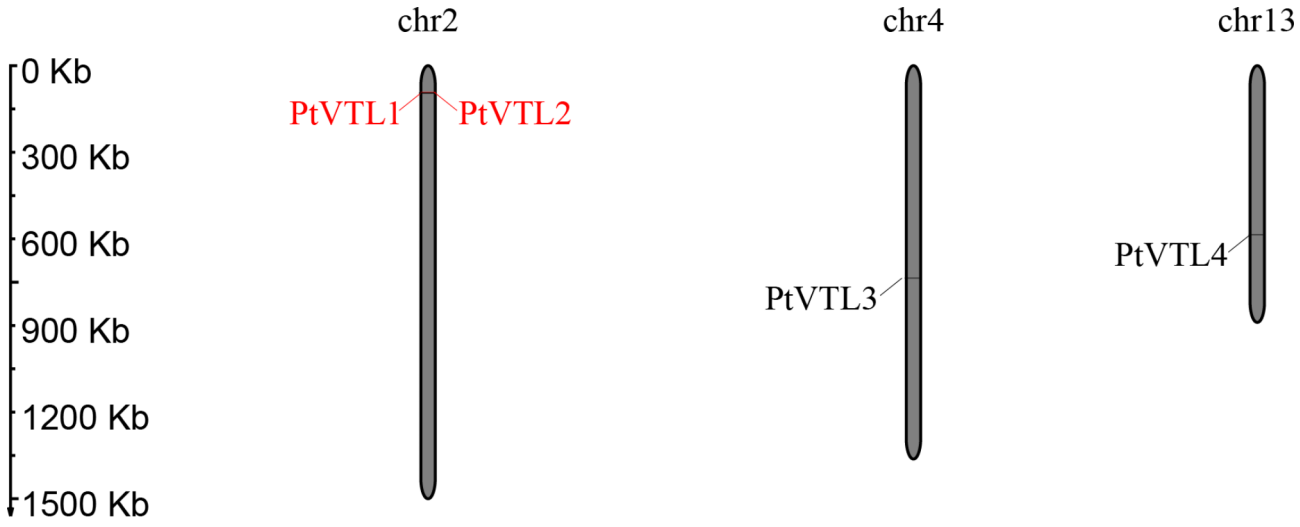

Fig. 3. Chromosome distribution of *PtVTL* genes. Red font represents the linked gene pair.

evolutionary pathway of PtVTL3 diverges from the other three PtVTLs, as it was not clustered with them in the VTL group.

Conserved motifs, domains, and gene structure of PtVTLs

To investigate the diversity of PtVTLs, we analyzed their conserved motifs. Our findings revealed five motifs associated with the VIT family (PF01988) in the PtVTLs (Supplementary Table 4). These motifs were arranged in the same order in PtVTL1, PtVTL2 and PtVTL4, whereas PtVTL3 only contained motif 2, 3 and 4. The characteristics of PtVTL3 were closely aligned with its phylogenetic relationships (Fig. 2A,B).

All PtVTLs contained the VIT family domain, which was localized on the C-terminus (Fig. 2C). The gene structure analysis indicated that only PtVTL4 contained one intron, while other three *PtVTL* genes were intronless (Fig. 2D).

Chromosomal distribution and gene duplication of *PtVTL* genes

Using the annotation file of the *P. tricornutum* genome, we employed the MG2C online program to visualize the distribution of *PtVTL* genes. The *PtVTL* genes were found on chromosomes: 2, 4, and 13, with *PtVTL1* and *PtVTL2* tightly linked on the same chromosome (Fig. 3). The distance between these two genes was only

Duplicated gene pair	Duplicated type	Ka	Ks	Ka/Ks	slection type
PtVTL1/ PtVTL2	Tandem	0.193473	0.513115	0.377057	Negative selection

Table 2. Ka/Ks ratio and duplicated date calculation for *PtVIT* genes. Ka/Ks < 1 means negative selection, Ka/Ks = 1 means neutral selection, and Ka/Ks > 1 means positive selection.

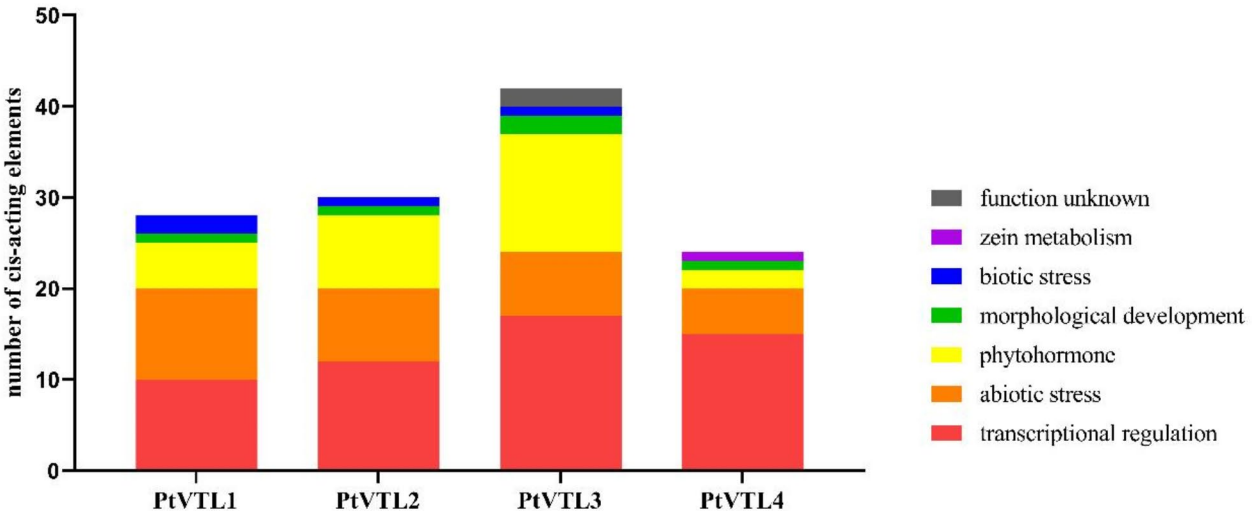

Fig. 4. Cis-acting regulatory elements analysis of *PtVTL* gene family. Red represents transcriptional regulation elements, orange represents abiotic stress responses elements, yellow represents phytohormone responses elements, green represents morphological development elements, blue represents biotic stress responses elements, purple represents zein metabolism responses elements, and gray represents function unknown responses elements.

772 bp (Table 1). A BLAST analysis revealed an identification rate of 88.49%, and 75% coverage between the two genes. This strongly suggests that the gene pair of *PtVTL1* and *PtVTL2* resulted from a gene tandem duplication event. We calculated the ratio of nonsynonymous substitutions per nonsynonymous site (Ka) to synonymous substitutions per synonymous site (Ks) of the *PtVTL1* and *PtVTL2* gene pair, finding that the Ka/Ks ratio was less than 1 (Table 2), indicating that this gene duplication event underwent negative selection[38].

Cis-acting regulatory elements and expression profile of *PtVTL* genes

Cis-acting elements in the promoter region can influence the precise and efficient expression of downstream genes. Given the gene density in the *P. tricornutum* genome[39], we extracted the 500 bp upstream sequence from the start codon of each gene for promoter analysis. In total, we identified 124 regulatory elements associated with *PtVTL* genes (Fig. 4). These elements were categorized into seven classes (included function unknown), and three classes occupy the vast majority: 54 elements for transcriptional regulation (Fig. 4, shown in red), 30 elements for abiotic stress responses (such as drought, light, and anoxic) (Fig. 4, shown in orange), and 28 elements related to phytohormone response (including abscisic acid, MeJA, jasmonic acid, auxin, and gibberellin) (Fig. 4, shown in yellow). Among these, CAAT-box (27) and TATA-box (7) were the most abundant regulatory elements for transcriptional regulation, while ABRE (7), as-1 (5), CGTCA-motif (5) and TGACG-motif (5) were the richest elements for phytohormone response. The G-Box (7), MYB (5), and MYC (4) elements were the most prevalent for abiotic stress. Notably, cis-acting elements related to transcription regulation, environmental stress, phytohormone response and morphological development were present in all *PtVTL* genes promoter regions, while elements associated with metabolism and biotic stress appeared only in some promoter regions. These findings suggest that the expression of *PtVTL* genes is predominantly regulated by environmental factors (e.g. light) and phytohormone. In addition, we try to seek some iron-responsive cis-elements, such as C(A/G)C(A/G)C(G/T)[40], A(A/C)G(G/C)C(G/-)C(A/G)TG, or CACGTG(T/C)C[41]. But regrettably, these iron-responsive cis-elements are not found.

To understand the roles of specific *PtVTL* genes at diel light cycling and different iron concentration, expression data for the four *PtVTL* genes were downloaded from the literature[32], and TBtools software was used to create HeatMap (Fig. 5). The results revealed that the expression of *PtVTL* genes were induced at different light condition. PtVTL3 was highly expressed under light, and others were highly expressed under dark condition, which might be associated with the cis-acting elements in the promoters. Specifically, *PtVTL2* was highly expressed at low iron conditions (20 pM Fe'), and *PtVTL3* exhibited high expression at high iron condition (400 pM Fe').

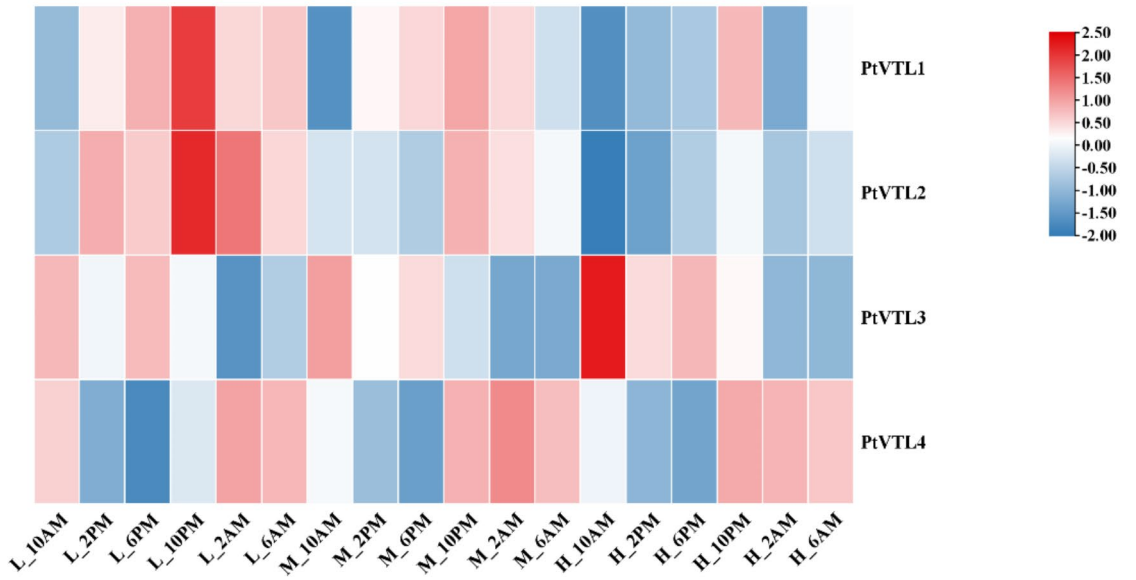

Fig. 5. The expression profile of *PtVTL* genes to diel light cycling (12:12) under iron limitation (standardized RPKM across Fe conditions). L: 20 pM Fe', M: 40 pM Fe', H: 400 pM Fe'. Fe': sum of all Fe species not complexed to EDTA. (data resource[32]:).

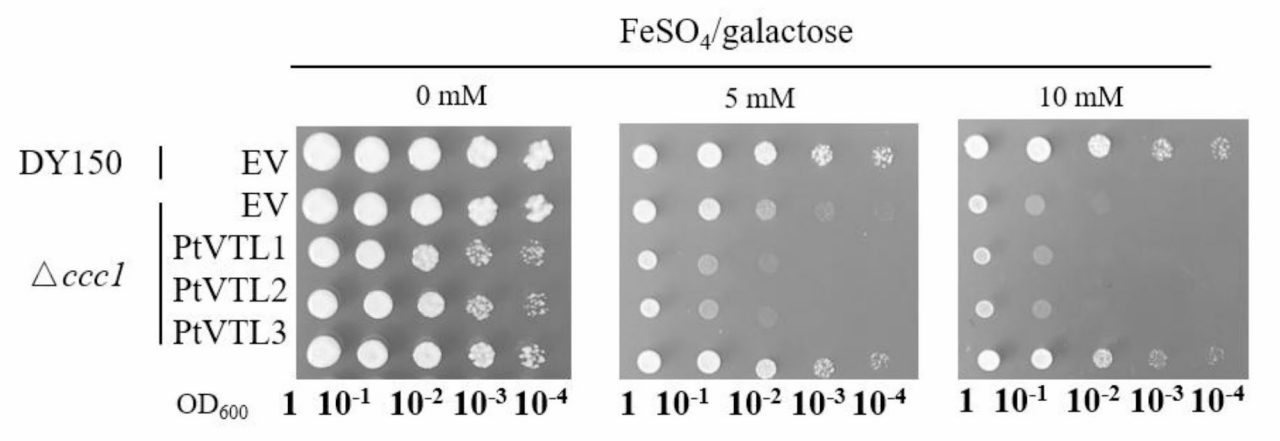

Fig. 6. The heterologous expression of *PtVTL* genes in yeast. Yeast wild type (WT) strain DY150 and mutant △*ccc1* cells containing pYES2 (EV), pYES2-PtVTL1, pYES2-PtVTL2 and pYES2-PtVTL3 grown on SGR medium without or with 5 and 10 mM $FeSO_4$ for 48hs and photographed. Each spot represents a 1:10 dilution of the culture starting with an OD of 1 on the far left (10-, 100-, and 100-fold dilutions).

Function analysis of PtVTLs

We amplified the *PtVTL* genes from the *P. tricornutum* strain CCMA 106 using RT-PCR, and the results indicated a premature stop code (TAA) at positions 100–102 bp in the *PtVTL4* gene, leading to early termination of translation. Therefore, we considered that PtVTL4 has not function in heavy metal transportation, and adopted *PtVTL1*, *PtVTL2* and *PtVTL3* to analysis the function of *PtVTLs*.

To assess the metal transport activity of PtVTLs, we conducted a yeast complementary assay. The *PtVTLs* (*PtVTL1*, *PtVTL2* and *PtVTL3*) were expressed in a yeast mutant strain, △*ccc1* (*Ca^{2+}-sensitive cross-complementer* 1 mutant), which is particularly sensitive to high extracellular Fe levels and fails to thrive in Fe enriched media[24]. The result demonstrated that *PtVTL3* successfully rescued the Fe^{2+} sensitivity in mutant △*ccc1*, indicating its role as an iron transporter (Fig. 6). But *PtVTL1* and *2* was not able to complement the Fe uptake mutant. PtVTL1 and 2 rescue mutants did not exhibit any growth differences after 48 h of growth on SGR medium containing 5 and 10 mM $FeSO_4$ compared with the mutant △*ccc1* cells. Interestingly, heterologous expression of *PtVTL3* in the Zn^{2+} uptake-defect mutant yeast △*Zrt1Zrt2* exhibited increased sensibility to 5 mM $ZnSO_4$ compared to the control. Conversely, the expression of *PtVTL3* in Mn^{2+} uptake-defective mutant yeast △*smf1* did not exhibit any

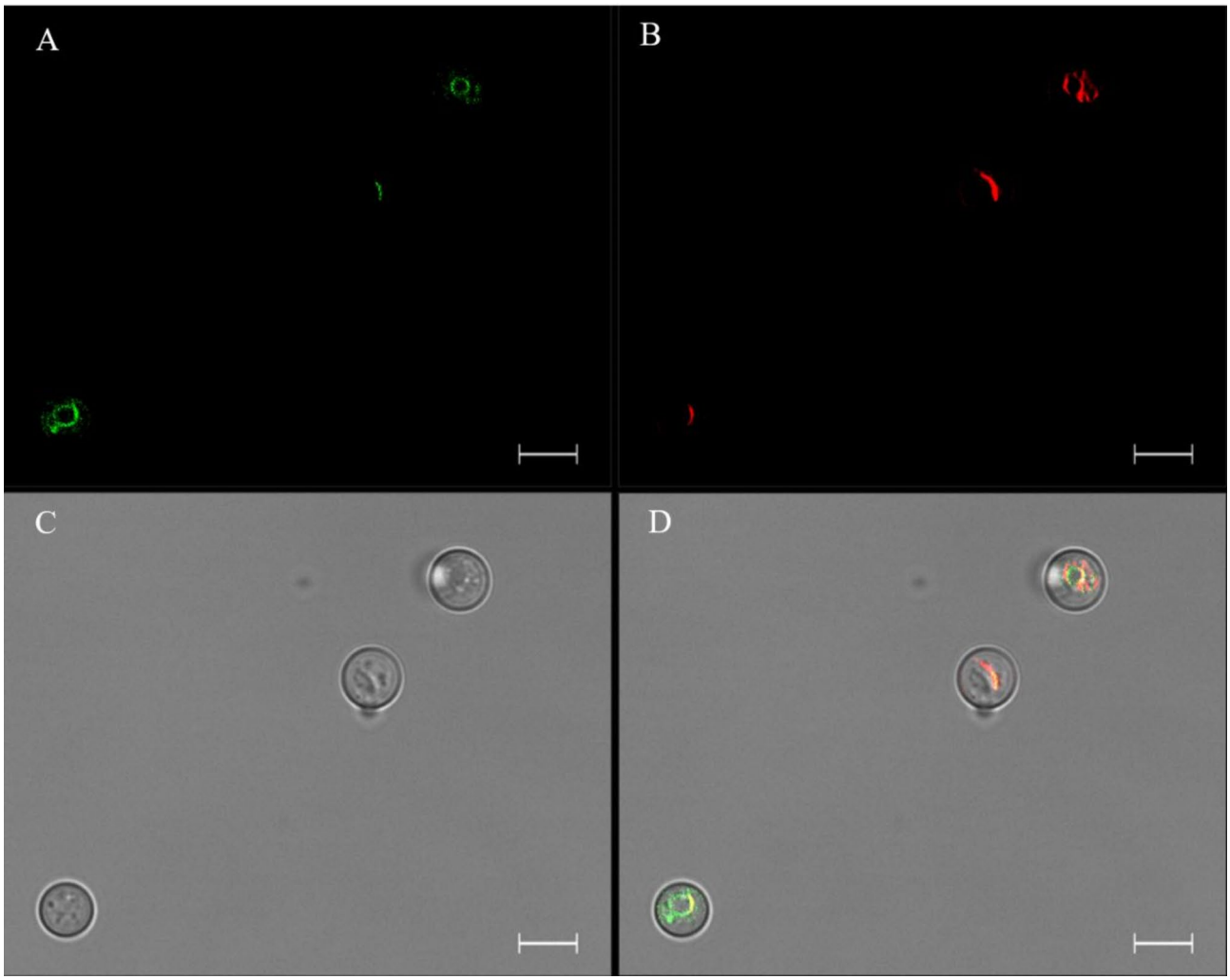

Fig. 7. Subcellular location of PtVTL3 in yeast mutant △*ccc1* cells. (**A**) eGFP-PtVIT3; (**B**) tonoplast fluorochrome FM4-64; (**C**) Bright Field; D: merged image. The green and red signal obtained with confocal microscopy indicated fusion protein eGFP-PtVIT3 and tonoplast fluorochrome FM4-64, respectively. The overlap image eGFP-PtVIT3 and FM4-64 signal is indicated in merged image. Bar = 5 μm.

growth differences compared to the control across various metal ion-enriched medium (Supplementary Fig. 1). And *PtVTL1* and *2* still appear to be unaffected by increased Zn^{2+} and Mn^{2+} concentrations.

The subcellular location of *PtVTL3* in yeast was observed using confocal microscope, and the images displayed that the eGFP-PtVTL3 fluorescence signal overlapped with the tonoplast fluorescence dye FM4-64 (Fig. 7), suggesting that the *PtVTL3* is primarily localized at the tonoplast.

Discussion

Saccharomyces cerevisiae CCC1, the first identified member of the VIT family, is located at the tonoplast, where it plays a crucial role in regulating the accumulation of iron and manganese within this organelle[24]. The overexpression of the CCC1 protein leads to a reduction in cytosolic iron concentration while increasing iron content in the vacuole. The first VIT protein discovered in plants was *Arabidopsis thaliana* AtVIT1, which shared 62% amino acid similarity with the yeast CCC1 protein. AtVIT1 is responsible for transporting iron into the vacuole under high-iron conditions, thereby supporting the normal development of *A. thaliana* seedling[34]. Similarly, *OsVIT1* and *OsVIT2* are located in the tonoplast and participate in the transport of Fe^{2+} and Zn^{2+} in rice[33]. OsVIT2, in particular, is expressed in the parenchyma cell bridges of nodes and play a significant role in distributing iron to grains by sequestering it into the vacuole within the mestome sheath, node, and aleurone layer[42]. In *Tulipa gesneriana*, the TgVIT1 protein is linked to iron accumulation in the blue-colored inner segments of petals, contributing to the blue pigmentation in purple cells[43–45]. Likewise, *Centaurea cyanus* CcVIT is involved in the blue coloration of cornflower petals[46].

In contrast to VIT proteins, VTL proteins lack a cytosolic loop in their tertiary structure, which serves as a metal-binding domain[17,36,47,48]. VTL proteins have been identified in both monocots and dicots, as well as in *Chlamydomonas* and *Physcomitrella*[35]. Overexpression of *A.thaliana AtVTL1*, *AtVTL2* or *AtVTL5* significantly

increased seed iron concentration in *nramp3*/*nramp4* or *vit1-1* mutants[35]. In *Medicago truncatula*, *MtVTL4* and *MtVTL8* were exclusively expressed in nodule, with MtVTL8 serving as the primary route for delivering iron to symbiotic rhizobia[36]. Similarly, in soybean (*Glycine max*), *GmVTL1a* and *GmVTL1b* are localized into the symbiosome membrane, with GmVTL1a facilitating iron transport across the membrane to bacteroids and playing a crucial role in the nitrogen-fixing symbiosis[37].

In this study, four members of the VIT family were identified in the genome of the marine diatom *Phaeodactylum tricornutum*. A phylogenetic tree constructed from different plant VIT family members revealed two distinct groups: the VIT group and the VTL group (Fig. 1), aligning with the phylogenetic trees created by Brear et al.[37] and Sharma et al.[49]. All four identified members belong to the VTL group.

Similar to findings in tomato and soybean[50], a gene duplication event was observed in the VIT family of *P. tricornutum*. The gene pair of *PtVTL1* and *PtVTL2* arose from tandem duplication, which is a key factor contributing to the expansion of this gens family in *P.tricornutum* (Fig. 3; Table 2).

The VIT family is involved in the transport of Fe^{2+}, Mn^{2+} and Zn^{2+}, regulating the homeostasis of these heavy metals within cells[19]. Like AtVTL1[35], GmVTL1a[51], MtVTL4 and MtVTL8[36], the heterogeneous expression of *PtVTL3* in yeast mutant $\triangle$*ccc1* was able to rescue growth under high Fe concentrations, indicating that PtVTL3 functions to transport Fe^{2+} and regulate iron homeostasis (Fig. 6). Additionally, we observed that in medium containing 5 mM $ZnSO_4$, the expression of *PtVTL3* in Zn^{2+}-sensitive yeast mutant $\triangle$*Zrt1Zrt2* exhibited increased Zn^{2+} sensitivity compared to the control (Supplementary Fig. 1), suggesting that PtVTL3 may also function as a bi-functional protein.

Like AtVTL1 and AtVTL2[34] and GmVTL1a[51], the eGFP-PtVTL3 fusion protein localized to the tonoplast in yeast (Fig. 7), which indicated that PtVTL3 may sequester Fe^{2+} into the vacuole for detoxification under high Fe^{2+} concentration conditions, thereby contributing to the regulation of iron homeostasis within cells.

Conclusions

In the genome of the marine diatom *Phaeodactylum tricornutum*, four members of the VIT gene family were identified, all of which belong to the VTL group. Each of the PtVTLs contains a VIT family domain, indicating a shared evolutionary origin. This gene family appears to have expansion through tandem duplication events. Based on the analysis of cis-acting regulatory elements, it is evident that PtVTLs play a role in responding to environmental stress and phytohormones, and the expression profile verified that *PtVTL3* gene was induced to express highly under light, and others were induced to express highly under dark condition. Specially, *PtVTL2* and *PtVTL3* genes were induced to express highly by low Fe and high Fe condition respectively. Additionally, the heterologous expression of *PtVTL3* in yeast mutant strain $\triangle$*ccc1* demonstrated that it is predominantly localized at the tonoplast, and is effective in rescuing yeast growth under the elevated iron concentrations.

Data availability

The data within the current manuscript are available from the corresponding author upon reasonable request.

Received: 7 September 2024; Accepted: 3 December 2024
Published online: 26 March 2025

References

1. Conte, S. S. & Walker, E. L. Transporters contributing to iron trafficking in plants. *Mol. Plant.* **4** (3), 464–476 (2011).
2. Burén, S. et al. Biosynthesis of nitrogenase cofactors. *Chem. Rev.* **120** (12), 4921–4968 (2020).
3. Botebol, H. et al. Central role for ferritin in the day/night regulation of iron homeostasis in marine phytoplankton. *Proc. Natl. Acad. Sci. U. S. A.* **112** (47), 14652–14657 (2015).
4. Behnke, J. & LaRoche, J. Iron uptake proteins in algae and the role of oron starvation-induced proteins (ISIPs). *Eur. J. Phycol.* **55** (3), 339–360 (2020).
5. Morel, F. M. M., Kustka, A. B. & Shaked, Y. The role of unchelated Fe in the iron nutrition of phytoplankton. *Limnol. Oceanogr.* **53** (1), 400–404 (2008).
6. Sutak, R., Camadro, J. M. & Lesuisse, E. Iron uptake mechanisms in marine phytoplankton. *Front. Microbiol.* **11**, 566691 (2020).
7. Gao, X., Bowler, C. & Kazamia, E. Iron metabolism strategies in diatoms. *J. Exp. Bot.* **72** (6), 2165–2180 (2021).
8. Morrissey, J. et al. A Novel protein, ubiquitous in marine phytoplankton, concentrates Iron at the cell surface and facilitates uptake. *Curr. Biol.* **25** (3), 364–371 (2015).
9. McQuaid, J. B. et al. Carbonate-sensitive phytotransferrin controls high-affinity iron uptake in diatoms. *Nature* **555** (7697), 534–537 (2018).
10. Allen, A. E. et al. Whole-cell response of the pennate diatom *Phaeodactylum tricornutum* to iron starvation. *Proc. Natl. Acad. Sci. U. S. A.* **105** (30), 10438–10443 (2008).
11. Kazamia, E. et al. Endocytosis-mediated siderophore uptake as a strategy for Fe acquisition in diatoms. *Sci. Adv.* **4** (5), eaar4536 (2018).
12. Coale, T. H. et al. Reduction-dependent siderophore assimilation in a model pennate diatom. *Proc. Natl. Acad. Sci. U. S. A.* **116** (47), 23609–23617 (2019).
13. Sutak, R. et al. A comparative study of iron uptake mechanisms in marine microalgae: iron binding at the cell surface is a critical step. *Plant. Physiol.* **160** (4), 2271–2284 (2012).
14. Tang, Z. et al. Molecular mechanisms underlying the toxicity and detoxification of trace metals and metalloids in plants. *J. Integr. Plant. Biol.* **65** (2), 570–593 (2023).
15. Connorton, J. M., Balk, J. & Rodriguez-Celma, J. Iron homeostasis in plants - a brief overview. *Metallomics* **9** (7), 813–823 (2017).
16. Liu, X. et al. Formation of resting cells is accompanied with enrichment of ferritin in marine diatom *Phaeodactylum tricornutum*. *Algal. Res.* **61**, 102567 (2022).
17. Ram, H., Sardar, S. & Gandass, N. Vacuolar iron transporter (like) proteins: regulators of cellular iron accumulation in plants. *Physiol. Plant.* **171** (4), 823–832 (2021).
18. Tan, X. et al. A review of plant vacuoles: formation, located proteins, and functions. *Plants* **8** (9), 327 (2019).
19. Sharma, S. S., Dietz, K. J. & Mimura, T. Vacuolar compartmentalization as indispensable component of heavy metal detoxification in plants. *Plant. Cell. Environ.* **39** (5), 1112–1126 (2016).

20. Potter, S. C. et al. HMMER web server: 2018 update. *Nucleic Acids Res.* **46** (W1), W200–W204 (2018).
21. Möller, S., Croning, M. D. R. & Apweiler, R. Evaluation of methods for the prediction of membrane spanning regions. *Bioinformatics* **17** (7), 646–653 (2001).
22. Kumar, S., Stecher, G. & Tamura, K. MEGA7: Molecular evolutionary genetics analysis version 7.0 for bigger datasets. *Mol. Biol. Evol.* **33** (7), 1870–1874 (2016).
23. Lapinskas, P. J., Lin, S. J. & Culotta, V. C. J. M. M. The role of the Saccharomyces cerevisiae CCC1 gene in the homeostasis of manganese ions. *Mol. Microbiol.* **21** (3), 519–528 (1996).
24. Li, L. et al. CCC1 is a transporter that mediates vacuolar iron storage in yeast. *J. Biol. Chem.* **276** (31), 29515–29519 (2001).
25. Fu, D., Beeler, T. & Dunn, T. *XII. Yeast sequencing reports. Sequence, mapping and disruption of CCC1, a gene that cross-complements the Ca2+-sensitive phenotype of csg1 mutants*. **10** (4) 515–521 (1994).
26. Letunic, I. & Bork, P. Interactive tree of life (iTOL) v5: an online tool for phylogenetic tree display and annotation. *Nucleic Acids Res.* **49** (W1), W293–W296 (2021).
27. Bailey, T. L. et al. The MEME suite. *Nucleic Acids Res.* **43** (W1), W39–49 (2015).
28. Wang, J. et al. The conserved domain database in 2023. *Nucleic Acids Res.* **51** (D1), D384–D388 (2022).
29. Chen, C. et al. TBtools: an integrative Toolkit developed for interactive analyses of big biological data. *Mol. Plant* **13** (8), 1194–1202 (2020).
30. Chao, J. et al. MapGene2Chrom, a tool to draw gene physical map based on Perl and SVG languages. *Hereditas* **37** (1), 91–97 (2015).
31. Lescot, M. et al. PlantCARE, a database of plant cis-acting regulatory elements and a portal to tools for in silico analysis of promoter sequences. *Nucleic Acids Res.* **30** (1), 325–327 (2002).
32. Smith, S. R. et al. Transcriptional orchestration of the global cellular response of a model pennate diatom to diel light cycling under iron limitation. *PLoS Genet.* **12** (12), e1006490 (2016).
33. Zhang, Y. et al. Vacuolar membrane transporters OsVIT1 and OsVIT2 modulate iron translocation between flag leaves and seeds in rice. *Plant. J.* **72** (3), 400–410 (2012).
34. Kim, S. A. et al. Localization of iron in Arabidopsis seed requires the vacuolar membrane transporter VIT1. *Science* **314** (5803), 1295–1298 (2006).
35. Gollhofer, J. et al. Vacuolar-iron-transporter1-like proteins mediate iron homeostasis in Arabidopsis. *PLoS ONE* **9** (10), e110468 (2014).
36. Walton, J. H. et al. The *Medicago truncatula* vacuolar iron transporter-like proteins VTL4 and VTL8 deliver iron to symbiotic bacteria at different stages of the infection process. *New. Phytol.* **228** (2), 651–666 (2020).
37. Brear, E. M. et al. GmVTL1a is an iron transporter on the symbiosome membrane of soybean with an important role in nitrogen fixation. *New. Phytol.* **228** (2), 667–681 (2020).
38. Hurst, L. D. The Ka/Ks ratio: diagnosing the form of sequence evolution. *Trends Genet.* **18** (9), 486–487 (2002).
39. Matthijs, M. et al. Profiling of the early nitrogen stress response in the diatom *Phaeodactylum tricornutum* reveals a novel family of ring-domain transcription factors. *Plant Physiol.* **170** (1), 489–498 (2016).
40. Deng and Eriksson. Two iron-responsive promoter elements control expression of FOX1 in *Chlamydomonas reinhardtii*. *Eukaryotic Cell* 2163–2167 (2007).
41. Yoshinaga, R. et al. Characterization of iron-responsive promoters in the marine diatom *Phaeodactylum tricornutum*. *Mar. Genom.* **16**, 55–62 (2014).
42. Che, J., Yamaji, N. & Ma, J. F. Role of a vacuolar iron transporter OsVIT2 in the distribution of iron to rice grains. *New. Phytol.* **230** (3), 1049–1062 (2021).
43. Momonoi, K. et al. A vacuolar iron transporter in tulip, TgVit1, is responsible for blue coloration in petal cells through iron accumulation. *Plant. J.* **59** (3), 437–447 (2009).
44. Momonoi, K. et al. Specific expression of the vacuolar iron transporter, TgVit, causes iron accumulation in blue-colored inner bottom segments of various tulip petals. *Biosci. Biotechnol. Biochem.* **76** (2), 319–325 (2012).
45. Shoji, K., Momonoi, K. & Tsuji, T. Alternative expression of vacuolar iron transporter and ferritin genes leads to blue/purple coloration of flowers in tulip cv. 'Murasakizuisho'. *Plant. Cell. Physiol.* **51** (2), 215–224 (2010).
46. Yoshida, K. & Negishi, T. The identification of a vacuolar iron transporter involved in the blue coloration of cornflower petals. *Phytochemistry* **94**, 60–67 (2013).
47. Sorribes-Dauden, R. et al. Structure and function of the vacuolar Ccc1/VIT1 family of iron transporters and its regulation in fungi. *Comput. Struct. Biotechnol. J.* **18**, 3712–3722 (2020).
48. Kato, T. et al. Crystal structure of plant vacuolar iron transporter VIT1. *Nat. Plants* **5** (3), 308–315 (2019).
49. Sharma, S. et al. Gene expression pattern of vacuolar-iron transporter-Like (VTL) genes in hexaploid wheat during metal stress. *Plants (Basel)* **9** (2), 229 (2020).
50. Cao, J. Molecular evolution of the vacuolar iron transporter (VIT) family genes in 14 plant species. *Genes* **10** (2), genes10020144 (2019).
51. Liu, S. et al. A VIT-like transporter facilitates iron transport into nodule symbiosomes for nitrogen fixation in soybean. *New. Phytol.* **226** (5), 1413–1428 (2020).

Acknowledgements

We appreciate professor Jiming Gong from the Chinese Academy of Sciences Center for Excellence in Molecular Plant Sciences, for the friendly giving of yeast wild type strain DY150 and mutant △ccc1 cells. In addition, we appreciate Dr. Jingting Zhang from Yangzhou University for the technical assistance in subcellular location research.

Author contributions

Rui Zhai, Xiangrui Zhang, and Zhiqi Zhang participated in vector construction and yeast complementation experiments. Shuying Wang, Yuhan Zhang, Dunwen Shi were mainly responsible for the data collection, analysis, and visualizaiton. Prof. Shuai Chen participated in the research of subcellular location. Guoqiang Chen designed the research and wrote the manuscript. Xinshu Li, Futian Li and Juntian Xu reviewed the manuscript.

Funding

This research received funding from Open-end Funds of Jiangsu Key Laboratory of Marine Biotechnology, Jiangsu Ocean University (HS2023003), Doctoral Research Initiation Fund of Jiangsu Ocean University (KQ21005), and the Priority Academic Program Development of Jiangsu Higher Education Institutions.

Declarations

Competing interests
The authors declare no competing interests.

Consent for publication
Authors are responsible for correctness of the statements provided in the manuscript.

Ethical approval and consent to participate
All data were collected from the public available databases on the internet. The experiments complied with current Chinese laws.

Additional information
Supplementary Information The online version contains supplementary material available at https://doi.org/10.1038/s41598-024-82161-9.

Correspondence and requests for materials should be addressed to G.C.

Reprints and permissions information is available at www.nature.com/reprints.

Publisher's note Springer Nature remains neutral with regard to jurisdictional claims in published maps and institutional affiliations.